Food Chemistry 319 (2020) 126544

Contents lists available at ScienceDirect

Food Chemistry

journal homepage: www.elsevier.com/locate/foodchem

Analytical Methods

A colorimetric biosensor for simultaneous ochratoxin A and aflatoxins B1 detection in agricultural products

Weiran Zhu[a,c], Liubo Li[d], Zhou Zhou[a], Xiaodi Yang[c], Nan Hao[a,*], Yingshu Guo[b,*], Kun Wang[a,*]

[a] Key Laboratory of Modern Agriculture Equipment and Technology, School of Chemistry and Chemical Engineering, Jiangsu University, Zhenjiang, Jiangsu 212013, PR China
[b] Shandong Province Key Laboratory of Detection Technology for Tumor Makers, School of Chemistry and Chemical Engineering, Linyi University, Linyi 276005, PR China
[c] College of Chemistry and Materials Science, Nanjing Normal University, Nanjing 210023, PR China
[d] Department of Interventional Oncology, Yueyang Hospital of Integrated Traditional Chinese & Western Medicine, Shanghai University of Traditional Chinese Medicine, Shanghai 200437, PR China

ARTICLE INFO

Keywords:
Colorimetric detection
Biosensor
Mycotoxin
Dual targets

ABSTRACT

Colorimetric biosensors have been widely applied to mycotoxins testing. However, the colorimetric assay previously reported used a single color to detect one mycotoxin, and there were few reports on the simultaneous detection of multiple mycotoxins. In this work, a colorimetric biosensor for dual mycotoxins detection was developed. A Fe_3O_4/GO based platform for aflatoxins B1 (AFB1) detection and a Fe_3O_4@Au based platform for ochratoxin A (OTA) detection were fabricated. The quantification of OTA and AFB1 was respectively achieved by the release of thymolphthalein under alkaline conditions and 3,3′,5,5′-tetramethylbenzidine was catalyzed by Au NPs under acidic conditions. Because of different conditions, two sensing methods didn't interfere with each other but could provide a higher detection efficiency. The detection range of AFB1 is 5–250 ng·ml^{-1} and that of OTA is 0.5–80 ng·ml^{-1}. This biosensor has been successfully applied in real sample detection, which has a broad application prospect in fields of food safety.

1. Introduction

Mycotoxins are toxic secondary metabolites produced by various fungi in proper temperature and humidity (Marin, Ramos, Cano-Sancho, & Sanchis, 2013). Food raw materials can be easily contaminated by mycotoxins during every process of food industry, including planting, growing, harvesting, storaging, transportation and processing. It will be a great threat to human health if mycotoxins enter into the food chain (Hussein & Brasel, 2001; Bennett & Klich, 2003). Therefore, various detection methods have been developed for mycotoxins detection, such as mass spectrometry (Sforza, Dall'asta, & Marchelli, 2006; Rubert, Soler, Marín, James, & Mañes, 2013), chromatography (Thomas, Wechsler, Chen, Crain, & Quilliam, 2016; Soleas, Yan, & Goldberg, 2001), enzyme-linked immunosorbent assay (ELISA) (Piermarini, Micheli, Ammida, Palleschi, & Moscone, 2007; Gordon Seymour, 2008), and fluorometry (Liu et al., 2015; Ligler et al., 2003; Medley et al., 2008). Although these instrumental analysis methods show excellent performances, the requirement of sophisticated equipment and well-trained operator is not friendly to less developed areas and hinders their applications to on-site detection. The development of simple, fast, sensitive detection methods for mycotoxins has become an important research topic for authorities and researchers in food safety (Shephard, 2008).

Colorimetric detection that transforms concentration information into color changes may be conducted by naked eyes (Song, Wei, & Qu, 2011). Owing to its low-cost, portability and easy-operation, colorimetric biosensor has been widely applied in daily life for various kinds of target detections, such as DNA (Liu et al., 2013; Fan et al., 2010), proteins (Fan et al., 2010; Xue et al., 2016), cells (Medley et al., 2008; Chen, Jackson, Rotello, & Nugen, 2016; Zhao et al., 2009), heavy metal ions (Zhang et al., 2015; Yu, Hong, Gao, & Nazeeruddin, 2016; Kim, Wen, Kim, & Yoon, 2012) and so on. There are also many previous works on colorimetric biosensors for mycotoxins detection. Common methods for such detections are to establish a quantitative relationship between the recognition of target objects and nanoparticles through the modification of nanoparticles, which in turn will lead to the color change of the solution, to achieve the target object detection purposes. For example, we developed a colorimetric aptamer biosensor for ochratoxin A (OTA) sensing based on the high peroxidase-like activity of gold nanoparticles (Au NPs) doped Fe_3O_4, which could catalyze

* Corresponding authors at: Tel.: +86 2583598493; +86 511 88791800.
E-mail addresses: hn@ujs.edu.cn (N. Hao), yingshug@126.com (Y. Guo), wangkun@ujs.edu.cn (K. Wang).

https://doi.org/10.1016/j.foodchem.2020.126544
Received 2 April 2019; Received in revised form 7 August 2019; Accepted 1 March 2020
Available online 02 March 2020
0308-8146/ © 2020 Elsevier Ltd. All rights reserved.

3,3′,5,5′-tetramethylbenzidine (TMB) with hydrogen peroxide. The solution color turned from colorless to blue and the target concentration was quantified by color intensity (Wang et al., 2016). Another popular approach is changing the dispersion status of noble metal nanomaterials. Due to the resonance of surface plasmon, the well dispersed or aggregated gold nanoparticles showed different colors from red to blue. Through a catalytic DNA circuit, an ultrasensitive detection of aflatoxin B1 (AFB1) was achieved with Au NPs as signal indicators (Chen, Wen, Zhuang, & Zhou, 2016).

As mentioned above, although there are different methods inducing the color change, most colorimetric biosensors can only detect one mycotoxin in one test because the quantification is based on a single color (Wang et al., 2016). Limited ability of multiplex detection disenables the simultaneous detection of various mycotoxins. In this work, whether it was feasible to combine two colorimetric methods into one to achieve dual target detection was explored. The quantification of OTA and AFB1 was respectively achieved by the catalysis of TMB under acidic conditions and the release of thymolphthalein (TP) under alkaline conditions. Because of different reaction conditions, two sensing methods didn't interfere with each other but could provide a higher detection efficiency. The detection range of AFB1 in this method is 5–250 ng·ml^{-1} and that of OTA is 0.5–80 ng·ml^{-1}.

2. Experimental section

2.1. Materials and apparatus

Diethylene glycol (DEG), ethylene glycol (EG), polyethylene glycol (PEG), $HAucl_4{\cdot}4H_2O$, tetraethylorthosilicate (TEOS), Tris (2-chloroethyl) phosphate (TCEP), Phosphate, thymolphthalein (TP), ferric chloride ($FeCl_3$) and ferrous sulfate ($FeSO_4{\cdot}7H_2O$) were purchased from Sinopharm Chemical Reagent Co. Ltd (China). Graphene oxide (GO) was purchased from Nanjing XFNANO Materials Tech Co. (3-aminopropyl) triethox-ysilane (APTS), OTA, fumonisin B1 (FB1) and AFB1 were purchased from Sigma-Aldrich. Semi-complementary AFB1 aptamer (DNA_1 and DNA_2) and AFB1 aptamer, Fluorescent dye labeled AFB1 aptamer (FOTA aptamer), OTA aptamer and the complementary of OTA aptamer (COTA aptamer) were obtained from Sangon Biotech Co. Ltd (China). Their sequences were shown in Table S1. Phosphate buffered saline (PBS, Na_2HPO_4-NaH_2PO_4, 0.1 M) was prepared in the laboratory and Doubly distilled water (18.2MΩ) was used throughout the experiment.

Atomic force microscopy (AFM) measurements were carried out with Bruker Innova Microscope instrument. Transmission electron microscopy (TEM) were performed on a JEOL 100 instrument (JEOL, Japan) at an accelerating voltage of 200 kV. Fluorescence spectra was recorded on a Hitachi F-4500 fluorescence spectra-photometer (Tokyo, Japan). UV–vis absorption spectra was characterized by spectrophotometer (UV-2450, Shimadzu, Japan). All the photos were taken by a Sony digital camera.

2.2. Basic principle

Firstly, Fe_3O_4/GO and TP-GO were combined with different AFB1′s semi-complementary chains respectively, then AFB1 aptamer was added and assembled to form AFB1 detection platform. Similarly, Fe_3O_4@Au and Au NPs were also combined with the semi-complementary chains and aptamer of OTA to form OTA detection platform. When AFB1 and OTA exist, both of the detection platform will dissociate because the affinity between the aptamer and the target is stronger than the semi-complementary chain. After magnetic separation, the supernatant was extracted for reaction and the amount of AFB1 and OTA was determined according to the color change of the corresponding solution under different pH values.

2.3. Sample preparation

The peanuts were completely ground by a high-speed disintegrator (Midea MJ WBL2501B). The shells would be removed from nuts before grinding the peanuts until the powdery consistencies were obtained.

A volume of 5 mL extraction solvent (ethanol/water, 80:20, v/v) was added to 2 g of ground sample in 10 mL centrifuge tube, then the sample was shaken with Vortex oscillator for 60 min at the speed of 1500 rpm at room temperature, followed by subsequent centrifugation for 8 min at 5000 rpm. 450 μL of supernatant was transferred and placed in a clean 2 mL centrifuge tube, followed by the additional 50 μL of the final concentration of AFB1 (10, 50, and 100 ng/ml) and OTA (1, 20, and 40 ng/ml) standard solution, and then the solution was shaken overnight to completely mix.

2.4. Procedures

2.4.1. Preparation for gold nanoparticles and Fe_3O_4/GO composite

Citrate-coated Au NPs were fabricated according to the traditional citrate reduction method (Huang et al., 2016; Huo et al., 2016). According to the previous method (Zhou et al., 2017; Hao, Lu, Zhou, Hua, & Wang, 2018), Fe_3O_4/GO nanocomposite was synthesized by in situ chemical co-precipitation of Fe^{2+} and Fe^{3+} in a basic solution in the presence of GO (Fe_3O_4 NPs were deposited on the surface of GO). The synthesis steps are as followed: 50 mL of GO (0.8 mg mL^{-1}) aqueous was processed by ultrasound for 1 h and N_2 was pumped into the aqueous for 30 min. Then, the aqueous solution (50 mL) of $FeCl_3$ (0.055 g) and $FeSO_4{\cdot}7H_2O$ (0.048 g) was purged with N_2 for 30 min. The mixed solution of Fe^{2+} and Fe^{3+} was added dropwise to the as-prepared GO suspension solution under magnetic stirring. To complete ion exchange, the mixed solution was stirred overnight in a nitrogen atmosphere. Then, in order to synthetize Fe_3O_4 magnetite nanocomposite by precipitation of Fe^{2+}/Fe^{3+} ions, the mixed solution was heated to 90 °C and the alkaline solution (NaOH, 6 M) was added dropwise to mixed solution and the pH of mixed solution was adjusted to 10.0. After stirring for 1.5 h, the solution cooled naturally. The as-prepared Fe_3O_4/GO solution was repeatedly washed to neutrality with PBS buffer (pH = 7.4) and was stored at 4 °C for further use.

2.4.2. Preparation for Fe_3O_4@Au magnetic beads (MBs)

The specific steps for the preparation for Fe_3O_4@Au are improved according to the methods previously reported in the literature (Zhou, Wei, Zhang, & Liu, 2013; Wang et al., 2015). The procedures are as followed: firstly, 30 mL of diethylene glycol (DEG) and 10 mL of ethylene glycol (EG) were mixed when stirring. 1 g of $FeCl_3{\cdot}6H_2O$ was later added to the above solution, and the mixture was stirred evenly. Next, 3 g of anhydrous sodium acetate was added into the above solution and was stirred for 30 min. Finally, 2 g of polyethylene glycol (PEG) was added and stirred for 40 min. The final solution was transferred to a 50 mL hydrothermal reaction vessel and maintained at 200 °C for 2 h. After the reaction, the reactor was taken out and cooled to room temperature. The product was subjected to magnetic separation and multiple ethanol washings to obtain pure Fe_3O_4 microspheres, which were re-dispersed with 50 mL of ethanol and stored at 4 °C until being used.

Mixture of 40 mL of the above prepared ethanol solution of Fe_3O_4 microspheres and 1 mL of 3-aminopropyltriethoxysilane (APTS) was stirred mechanically for 10 h, which was magnetically separated and washed with ethanol several times. After magnetic separation, solids were re-dispersed into 40 mL of water and placed in a three-necked flask; Next, 3 mL of $HAuCl_4$ solution (2 wt%) was added slowly and refluxed at 100 °C for 50 min, and then 6 mL of trisodium citrate (2 wt %) was added dropwise to the mixture. Such a reaction was refluxed under boiling for 3 h (Au NPs were deposited on the surface of Fe_3O_4). After magnetic separation and ultrapure water washing several times, pure Fe_3O_4@Au MBs were re-dispersed with 40 mL of water and stored

at 4 °C for further use.

2.4.3. Preparation for Au NPs-OTA aptamer

The 5 OD OTA aptamer was activated with 240 μL of 100 μM trichloroethyl phosphate (TCEP), and then the OTA aptamer solution was added to 35 mL Au NPs dispersion prepared before and sonicated for 0.5 min to make the OTA aptamer well dispersed (Wang, Shan, Zhao, Xu, & Chen, 2011). After oscillating the reaction at 37 °C for 1 h, 0.5 M, 1.0 M, 1.5 M and 2.0 M NaCl solutions was added and centrifuged at 14,000 r and washed with 0.01 M PBS buffer to remove extra OTA aptamer. Next, 35 mL of 6-mercaptohexanol (MCH) at a concentration of 1 μM was added to the Au NPs and shaken continually at 37 °C for 1 h. The mixture was centrifuged and washed several times with 0.01 M PBS buffer, and the resulting Au NPs-OTA aptamer was re-dispersed in 35 mL PBS buffer and stored at 4 °C until being used (OTA aptamer and Au NPs are covalently bound by Au-S). The method of preparation for Fe_3O_4@Au-COTA aptamer was similar as that of Au NPs-OTA aptamer, and the difference was replacing Au NPs with Fe_3O_4@Au. In brief, after NaCl was added, the solution was magnetically separated and washed with 0.01 M PBS buffer to remove extra COTA aptamer. Next, 20 mL of MCH (2 μM) was added to the magnetic separated solid, shaking continually for 1 h. Then the mixture was magnetically separated and washed several times with 0.01 M PBS buffer. Then the resulting Fe_3O_4@Au-COTA aptamer was re-dispersed in 20 mL PBS buffer and stored at 4 °C for use.

2.4.4. Preparation for Au NPs-OTA aptamer-Fe_3O_4@Au-COTA aptamer nanocomposites

The above prepared Au NPs-OTA aptamer dispersion was mixed with the Fe_3O_4@Au-COTA aptamer dispersion. After shaking the reaction at 37 °C for 2 h, the OTA aptamer and its complementary strand COTA aptamer would hybridize and couple (Base pairs are complementary), then magnetic separation and multiple washings with PBS buffer, Au NPs-OTA aptamer- Fe_3O_4@Au-COTA aptamer nanocomplexes were obtained and re-dispersed in 20 mL PBS buffer, stored at 4 °C until being used. The assembly diagram is as shown in Fig. 1A.

2.4.5. Preparation for TP-DNA_1-GO

At room temperature, the GO aqueous solution (1 mL) was removed and sonicated for 2 h. DNA_1 solution dissolved in PBS buffer (0.01 M) was added and shaken for 22 h, then it was centrifuged and washed for three times with PBS buffer. Then 900 μL of PBS buffer and 100 μL of thymolphthalein (TP) in ethanol were added and shaken for 3 h, centrifuged and washed for three times with PBS buffer to obtain TP-DNA_1-GO and then re-dispersed in 1 mL of PBS buffer and stored at 4 °C until being used.

2.4.6. Preparation for DNA_2-Fe_3O_4/GO

DNA_2 solution was added into 1 mL of the above prepared Fe_3O_4/GO solution and shaken for 22 h, centrifuged and washed for three times with PBS buffer to obtain DNA_2-Fe_3O_4/GO and then re-dispersed in 1 mL of PBS buffer.

2.4.7. Preparation for TP-DNA_1-GO-AFB1 aptamer-DNA_2-Fe_3O_4/GO

500 μL of PP-DNA_1-GO and 500 μL of DNA_2-Fe_3O_4/GO were mixed. 50 μL of the AFB1 aptamer was added into the mixture and shaken for 12 h. DNA_1 and DNA_2 are two ssDNAs that are partially complementary to the AFB1 aptamer. When the two platforms are mixed with the AFB1 aptamer in solution, DNA_1 and DNA_2 are simultaneously hybridized with the AFB1 aptamer to form TP-DNA_1-GO-AFB1 aptamer-DNA_2-Fe_3O_4/GO assembly. After magnetically separated and washed with PBS buffer for three times, TP-DNA_1-GO-AFB1 aptamer-DNA_2- Fe_3O_4/GO was obtained and stored at 4 °C for AFB1 detection. The assembly diagram is as shown in Fig. 1B.

2.4.8. Simultaneous dual target detection of AFB1 and OTA

Pipetting 1 mL of TP-DNA_1-GO-AFB1 aptamer-DNA_2-Fe_3O_4/GO and

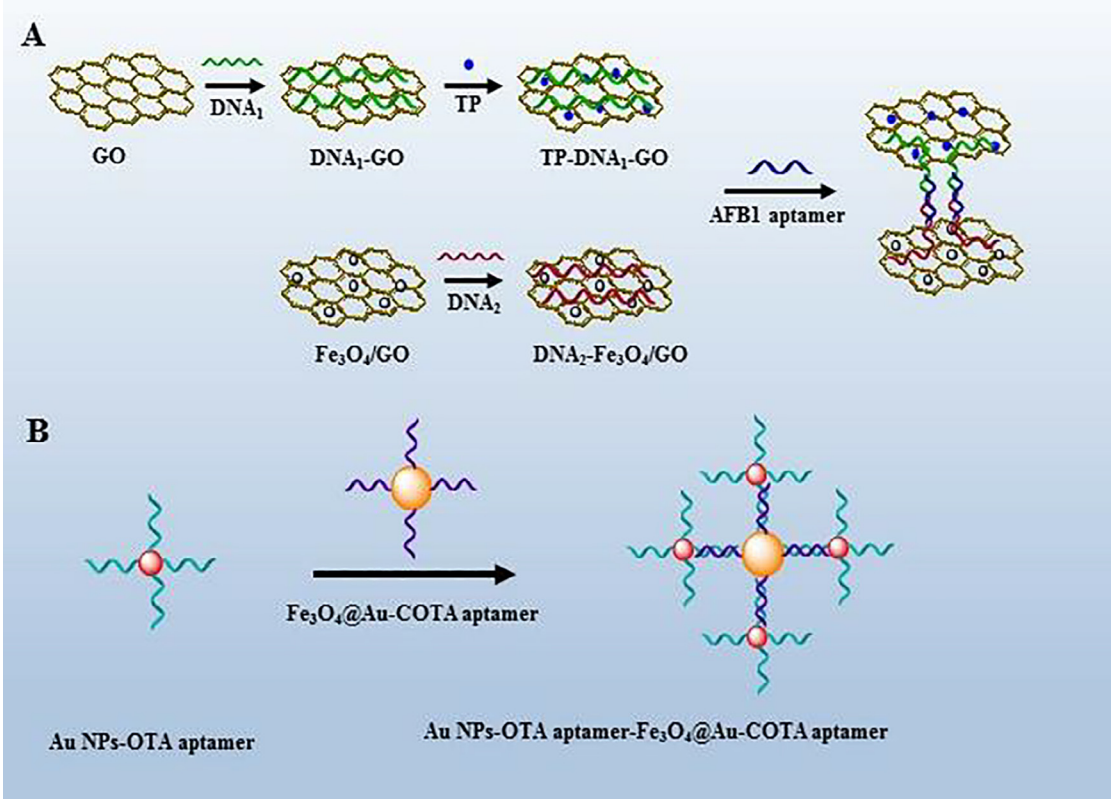

Fig. 1. The assembly diagram of (A) TP-DNA_1-GO-AFB1 aptamer-DNA_2-Fe_3O_4/GO (B) Au NPs-OTA aptamer-Fe_3O_4@Au-COTA aptamer Nanocomposites.

200 μL of Au NPs-OTA aptamer-Fe_3O_4@Au-COTA aptamer into a centrifuge tube, removing the supernatant after magnetic separation. 200 μL of PBS buffer with different concentrations of AFB1 and OTA was added to the centrifuge tube and incubated at 37 °C for 90 min with shaking. By magnetic separation, the alkaline solution was then added to the magnetic separated solids, the pH of the solution was brought to 12.0, and the solution was shaken for 5 min at room temperature. The absorbance of the above solution was measured by an UV–vis spectrophotometer. A standard curve was established based on the relationship between the intensity of the absorption peak and the concentration of the corresponding AFB1 standard. At the same time, 100 μL of the supernatant after magnetic separation was removed, 400 μL of PBS buffer (0.01 M) was added and the pH was adjusted to 4.0, and then 200 μL of H_2O_2 and 100 μL of TMB were added for color development. The reaction was conducted while shaking at 40 °C for 10 min and the reaction was stopped after adding 100 μL of 2 M H_2SO_4. The absorbance of the above solution was measured by an ultraviolet spectrophotometer and its corresponding photograph was taken. A standard curve was established based on the relationship between the intensity of the ultraviolet absorption peak and the corresponding OTA standard concentration.

3. Results and discussion

3.1. Detection principle and verification

The detection principle of this biosensor is shown in Fig. 2, which consists of a Fe_3O_4/GO based platform for AFB1 and a Fe_3O_4@Au based platform for OTA. Fe_3O_4/GO and TP-GO formed the platform through the combination of AFB1 aptamer. Fe_3O_4@Au and Au NPs formed the platform through the complementary strands of OTA aptamer and probe. The two platforms could be easily separated by magnetic separation without AFB1 and OTA, and the supernatant was colorless. When the alkaline solution was added to the magnetically separated solids, the solution was dark blue due to the release of TP; when the supernatant was used to catalyze TMB, the solution was colorless because of the absence of Au NPs. When both AFB1 and OTA were present, they would bind with corresponding aptamers and caused the dissociation of two platforms. Therefore, only Fe_3O_4/GO and Fe_3O_4@Au could be magnetically separated. Since TP-GO and Au NPs remained in the supernatant, when alkaline solution was added to the magnetically separated solid, the color of the solution wouldn't change into blue without the presence of TP. Au NPs in the supernatant could catalyze the coloration of TMB, and the color of the solution changed from colorless to blue as the concentration of OTA increased.

AFM was applied to investigate structural changes during reaction processes. As shown in Fig. 3A, the bare GO plate was around 1.3 nm thick. After mixing the DNA_1-GO and DNA_2-Fe_3O_4/GO complexes with AFB1 aptamer, large aggregates were observed in the AFM due to the hybridization of DNA_1 and DNA_2 with AFB1 aptamer (Fig. 3B). The thickness of the slice indicated that the DNA self-assembled GO assembly was around 19.2 nm, which was in accordance with DNA-assembled nanosheet multilayers.

3.2. Characterization of Fe_3O_4/GO nanomaterials

To verify the synthesis of Fe_3O_4/GO nanomaterials, the morphology and structure of GO and Fe_3O_4/GO nanomaterials were investigated by transmission electron microscopy (TEM). Fig. S1A shows a representative view of GO nanosheets, revealing the stacking and the corrugated structure, which shows that GO has a large specific surface area and great advantages for modifying magnetic nanoparticles. Fig. S1B shows the TEM images of the prepared Fe_3O_4/GO nanocomposites, clearly revealing that the two-dimensional GO nanosheets are modified by many Fe_3O_4 nanoparticles on the surface. Compared to the Fe_3O_4, although the saturation magnetization of Fe_3O_4/GO is lowered, attributed to the contribution of the overall mass of the non-magnetic GO, it did not affect the magnetic separation of Fe_3O_4/GO as a whole (Zhang et al., 2015). As can be seen from Fig. S1C, since the Fe_3O_4 nanoparticles are modified on the surface, the resulting Fe_3O_4/GO can be rapidly separated by the magnet (b in Fig. S1C) and rapidly re-dispersed by hand vibration.

3.3. Characterization of GO and Fe_3O_4/GO labeled nano-biological probes

From the fluorescence spectrum in Fig. S2, it can be seen that the fluorescent molecule-labeled AFB1 aptamer (FAFB1 aptamer) has strong fluorescence in PBS buffer. When GO and Fe_3O_4/GO were added to the solution, the fluorescence performance disappeared. The fluorescence quenching is contributed to the electron or energy transferring between the FAM and GO surface. This result demonstrated that single-stranded DNA (ssDNA) could bind on GO and Fe_3O_4/GO with a strong interaction affinity (Tang, Wang, Liu, & Li, 2011).

As can be observed from Fig. 4A, GO, DNA_1-GO and TP-DNA_1-GO have the same color, yellow–brown. After adding alkaline solution (pH 12.0) to the three solutions, the TP-DNA_1-GO complex turned blue, which demonstrated that the TP molecule was released from GO surface and caused color changes in the alkaline condition. This phenomenon is attributed to the transition of TP from a colorless internal lipid structure to a quinoid structure. Such a color change is accompanied by spectra changes at 294, 383, and 594 nm (Fig. 4B). It is also worth noting that there is no color change in the supernatant after centrifugation of TP-

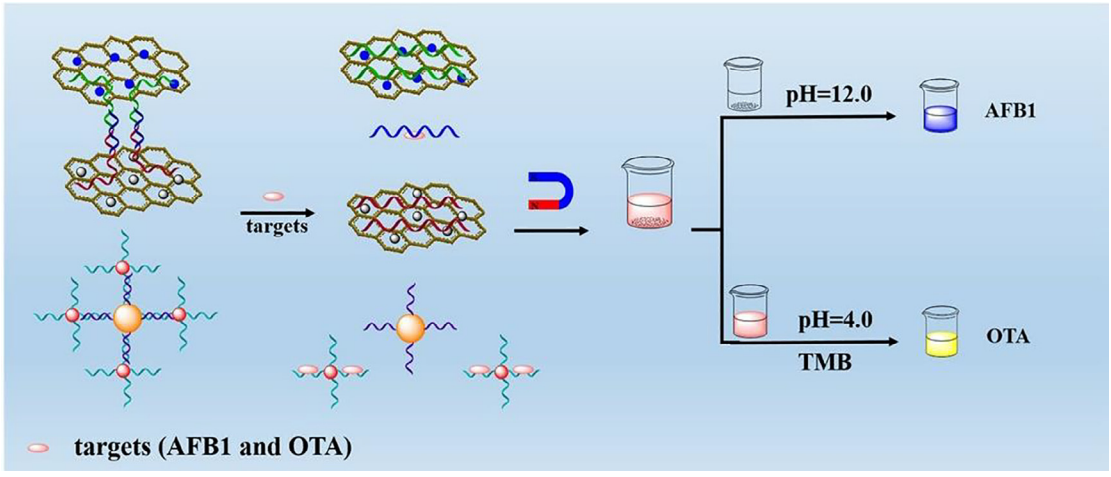

Fig. 2. The working principle for AFB1 and OTA detection based on colorimetric biosensor.

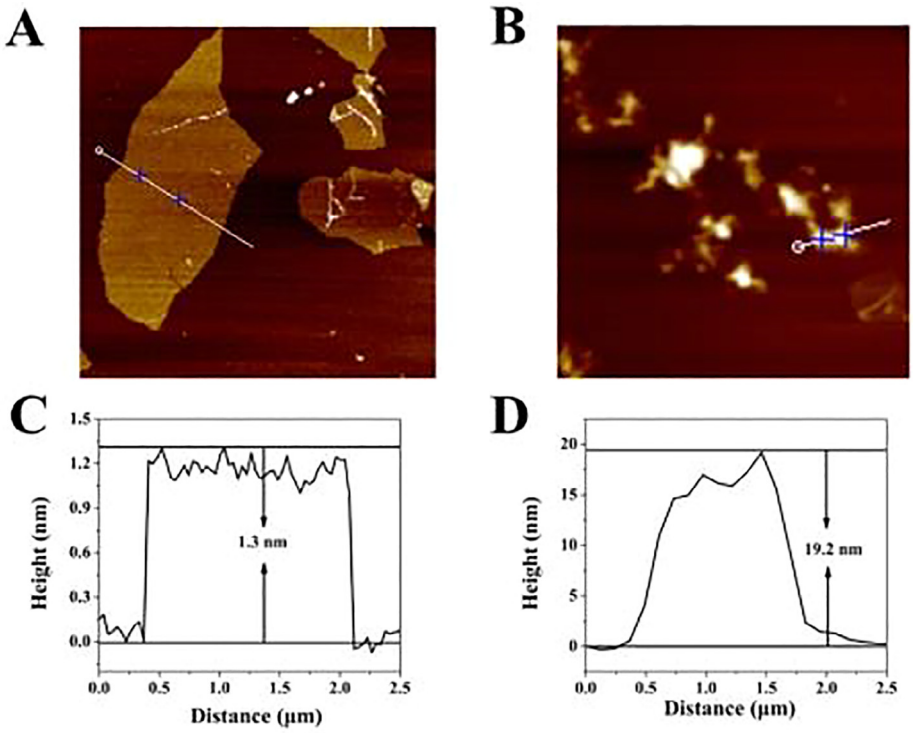

Fig. 3. AFM images and height profiles of (A) bare GO, (B) DNA_1-GO-AFB1 aptamer-DNA_2-GO on freshly cleaved mica.

DNA_1-GO. This shows that the leakage of TP can be ignored.

3.4. Characterization of Au NPs and Au NPs-OTA aptamers

From Fig. S3A, it can be seen that the synthesized Au NPs are wine red and the maximum absorption peak is at 522 nm (curve a), indicating that Au NPs have been successfully synthesized. In addition, the TEM image shows that the diameter of Au NPs is about 20 nm (Fig. S3B). Thiol group functionalized OTA aptamer was applied to modify Au NPs in this experiment through Au-S bond. Compared with the UV–vis absorption spectra of Au NPs (Fig. S3A, curve a), Au NPs-OTA aptamer (Fig. S3A, curve c) shows a new absorption peak around 260 nm, which is consistent with the position of the free OTA aptamer absorption peak (Fig. S3A, curve b) and indicates that the OTA aptamer is successfully modified (Peng, Li, Mu, & Guo, 2013).

3.5. Characterization of Fe_3O_4@Au and Fe_3O_4@Au-COTA aptamer

From the TEM image of Fe_3O_4 (Fig. 5A), it can be seen that Fe_3O_4 has a spherical structure with an average diameter of about 250 nm. Compared with Fe_3O_4, the diameter of Fe_3O_4@Au is obviously increased about 300 nm (Fig. 5B). And a clear core–shell structure indicates the successful preparation of Fe_3O_4 and Fe_3O_4@Au (Xu, Hou, & Sun, 2007). Fig. 5C shows the absorption spectra of Fe_3O_4 (a) and Fe_3O_4@Au (b). Fe_3O_4 has no obvious absorption peak, while Fe_3O_4@Au has an obvious absorption peak at 410 nm. The color of Fe_3O_4 aqueous solution is black, while that of Fe_3O_4@Au aqueous solution is khaki. The Fe_3O_4@Au aqueous solution can be separated within 15 s under the applied magnetic field and can be re-dispersed under slight oscillation. As can be seen from Fig. 5D, COTA aptamer modified with -SH was successfully attached to the surface of Fe_3O_4@Au via Au-S bond, indicating that Fe_3O_4@Au-COTA aptamer was successfully prepared (Freeman et al., 1995).

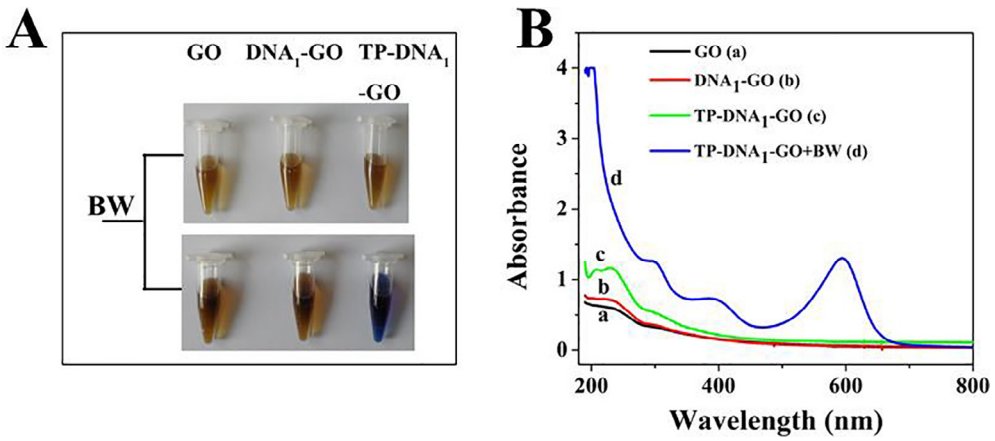

Fig. 4. (A) Bright-field images of solutions containing GO, DNA_1-GO, and TP-DNA_1-GO before and after treating with BW (pH 12.0). (B) Absorption spectra of solutions containing GO (a), DNA_1-GO (b), TP-DNA_1-GO (c), and TP-DNA_1-GO (d) treated with BW (pH 12.0).

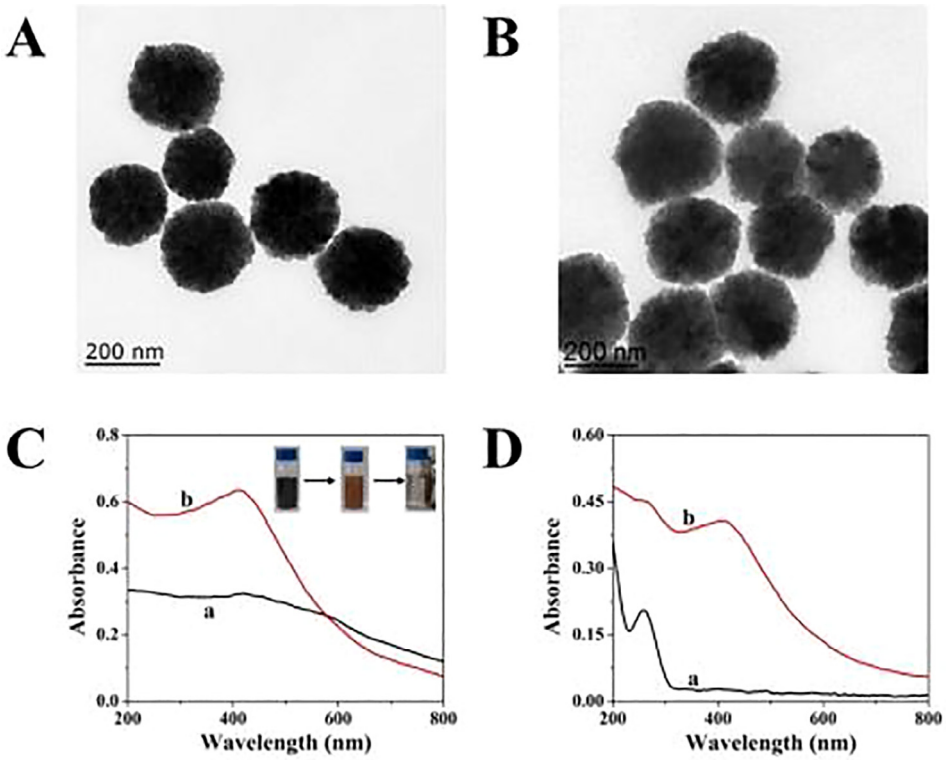

Fig. 5. TEM images of theFe_3O_4 (A) and Fe_3O_4@Au (B), (C) the UV–vis spectra of Fe_3O_4 (a) and Fe_3O_4@Au (b), (D) the UV–vis spectra of free COTA aptamer (a) and Fe_3O_4@Au- COTA aptamer (b).

3.6. Study on Au NPs peroxidase

In order to study the peroxidase activity of Au NPs, the catalytic activity of Au NPs was studied under different systems with TMB as the color reaction substrated. As can be seen from Fig. S4, when Au NPs and H_2O_2 or TMB are present, the color of the solution does not change after the reaction. Only H_2O_2 and TMB exist together. Au NPs can catalyze the oxidation of TMB by H_2O_2 to produce a blue color, and the maximum absorption peak appears at 655 nm. Because H_2O_2 can be adsorbed on the surface of Au NPs, and the O—O bond of H_2O_2 broke up into double HO· radical. The generated HO· might be stabilized by Au NPs via the partial electron exchange interaction, oxidizing TMB to make the solution blue (Jv, Li, & Cao, 2010).

The peroxidase activity of Au NPs is very sensitive to the temperature of the reaction medium, pH and H_2O_2 concentration (Ni et al., 2014). The activity of Au NPs peroxidases was evaluated at different temperatures. Fig. S5A shows that the highest catalytic activity is obtained at 40 ˚C. As shown in Fig. S5B, Au NPs have the greatest catalytic activity at a pH of 4.0 by changing the pH of the reaction medium from 2.0 to 7.0. The catalytic time was also optimized from 2 min to 14 min. It can be seen from Fig. S5C that after the catalytic time reaches 10 min, the absorption peak intensity reaches a plateau, which indicates that the catalytic reaction has ended at 10 min. As shown in Fig. S5D, the H_2O_2 concentration is optimized as well and the concentration of H_2O_2 at 0.7 M is chosen. We also performed an orthogonal analysis of the four factors affecting Au-catalyzed TMB. As shown in Table S2, pH values and temperature have more significant effects on the reaction.

3.7. Optimization of experimental condition

Experimental conditions were optimized in order to increase the detection sensitivity. Firstly, the reaction temperatures of the AFB1 and OTA assays were studied. The absorption spectra responses of the magnetically separated solid treated with BW (pH = 12.0) and the supernatant catalyzed TMB under the different reaction temperatures were shown in Fig. S6A. The optimum incubation temperature for detecting AFB1 and OTA was 37 ˚C. Because the absorption peak intensity of the solid particle solution at this temperature was minimum, while that of the supernatant catalyzed TMB was maximum. Secondly, reaction time was controlled in the range of 10–120 min (Fig. S6B). In the early stages of the reaction, the peak intensity of solid particle solution decreased for 90 min. Over 90 min of incubation time, the absorption intensity reached a plateau. And the absorption peak intensity of the supernatant catalyzed TMB solution increased for 60 min. From the above results, the optimal incubation time for the following tests was chosen as 90 min.

3.8. Simultaneous colorimetric detection of AFB1 and OTA

By combining two methods, a simple, rapid, and sensitive dual-methods colorimetric biosensor was developed at this temperature. Taking AFB1 and OTA as examples, the detection performance was demonstrated. AFB1 and OTA solutions with different concentrations were added to the solution containing TP-GO-AFB1 aptamer-Fe_3O_4/GO and Au NPs-OTA aptamer-Fe_3O_4@Au. Then the solution color changed according to different target concentrations. As shown in Fig. 6, the color of the precipitated solution gradually changed from blue to colorless, and the peak of absorption intensity at 594 nm gradually decreased as the concentrations of AFB1 increased (Fig. 6A). Fig. 6B shows the linear relationship between the absorption peak intensity and the AFB1 concentrations from 5 to 250 ng·mL^{-1}. After TMB was catalyzed by the supernatant, the color changed from colorless to yellow as the concentration of OTA increased. As shown in Fig. 6C, the peak intensity at 450 nm increased and the yellow color became deeper. Fig. 6D shows the peak intensity is linearly related to OTA concentrations in the range of 0.5–80 ng·mL^{-1}.

Control experiments were also performed to evaluate the selectivity. The sensing results of blank (no AFB1 and OTA), AFB1, OTA, FB1, AFB1 + OTA, and AFB1 + OTA + FB1 is shown in Fig. S7. The response from FB1 was negligible at the concentration of 200 ng·mL^{-1}.

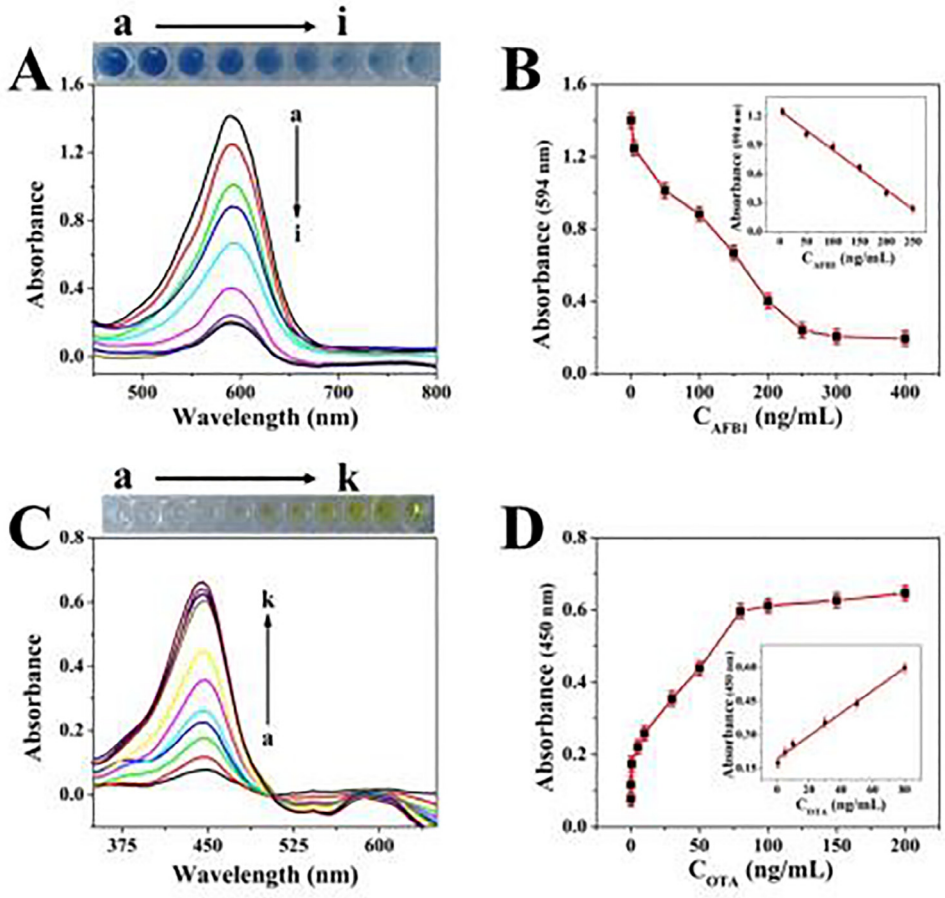

Fig. 6. (A) The picture and the UV–vis absorption intensity of the solution after adding different concentrations of AFB1 after magnetic separation of solids were treated with BW (pH = 12.0). (B) The response curve between the peak absorption at 594 nm with AFB1concentrations. Inset shows the linearity of the assay at the AFB1 concentrations range of 5–250 ng·mL^{-1}. (C) The picture and the UV–vis absorption intensity of the solution after catalyzing TMB by the supernatant with different concentrations of OTA. (D) The response curve between the peak absorption at 450 nm with OTA concentrations. Inset shows the linearity of the assay at the OTA concentrations range of 0.5–80 ng·mL^{-1}.

AFB1 could only affect the absorption peak at 594 nm, and OTA could only affect the absorption peak at 450 nm (the concentrations of AFB1 and OTA are 100 ng·mL^{-1} and 50 ng·mL^{-1}, respectively). The above result reveals that this biosensor can well discriminate different toxins.

In order to further study the applicability of actual sample analysis of the constructed dual-method biosensor, the content of AFB1 and OTA in peanuts and barley was determined with present method and high-performance liquid chromatography (HPLC). Through recording the corresponding UV–vis absorption intensity of the solution and substituting them in the linear formula, the test values were calculated and the recoveries were further obtained. As shown in Table 1, the recovery rate was achieved in the range of 87.3–102.5% (n = 3) and the RSD was in the range of 4.7% to 8.4%, Compared to the standard method HPLC, this sensor shows not inferior detection capability and stability, which indicated that this biosensor could be used for the detection of AFB1 and OTA in real samples. Furthermore, a comparison of the developed method in this work with other published colorimetric methods for the detection of OTA and AFB1 are presented in Tables S3 and S4.

Table 1
Comparison of AFB1 and OTA detection results by different methods.

Sample	Target	Added (ng·mL^{-1})	Found (ng·mL^{-1})	Recovery (%)	RSD (%)	Method
Peanut	AFB1	50.0	46.3	92.6	5.8	This
Barley	OTA	20.0	20.5	102.5	6.3	This
Barley	AFB1	100.0	96.4	96.4	8.4	This
Peanut	OTA	40.0	34.9	87.3	4.7	This
Peanut	AFB1	50.0	44.7	89.4	6.2	HPLC
Barley	OTA	20.0	19.2	96.0	7.8	HPLC
Barley	AFB1	100.0	93.7	93.7	3.9	HPLC
Peanut	OTA	40.0	36.5	91.2	4.5	HPLC

4. Conclusions

In conclusion, a biosensor for simultaneous dual target detection has been successfully developed with the combination of two colorimetric methods. Two targets, OTA and AFB1, may be respectively quantified by the catalysis of TMB under acidic conditions and the release of TP under alkaline conditions. Because of different reaction conditions, two sensing methods didn't interfere with each other but could even provide a higher detection efficiency. This developed biosensor shows good detection performance with linear ranges of AFB1 5–250 ng·mL^{-1} and OTA 0.5–80 ng·mL^{-1} besides a good reproducibility and selectivity, which has a broad application prospect in fields of food safety and environmental monitoring.

Declaration of Competing Interest

The authors declare that they have no known competing financial interests or personal relationships that could have appeared to influence the work reported in this paper.

Acknowledgments

This work was supported by grants from the National Key Research and Development Plan (No. 2017YFD0200303), National Natural Science Foundation of China (Nos. 21876068, 21505055, and 21675066), Natural Science Foundation of Jiangsu Province (No. BK20150486), China Postdoctoral Science Foundation funded project (2017M621652), Special Foundation of China Postdoctoral (2018T110456), Postdoctoral Science Foundation funded project of Jiangsu province (1701075C), and Jiangsu Provincial Engineering Laboratory for Advanced Materials of Salt Chemical Industry

(SF201703).

Appendix A. Supplementary data

Supplementary data to this article can be found online at https://doi.org/10.1016/j.foodchem.2020.126544.

References

Bennett, J. W., & Klich, M. (2003). Mycotoxins. *Clinical Microbiology Reviews, 16*(3), 497-+.

Chen, J., Jackson, A. A., Rotello, V. M., & Nugen, S. R. (2016). Colorimetric Detection of Escherichia coli Based on the Enzyme-induced Metallization of Gold Nanorods. *Small (Weinheim an der Bergstrasse, Germany), 12*(18), 2469–2475.

Chen, J., Wen, J., Zhuang, L., & Zhou, S. (2016). An enzyme-free catalytic DNA circuit for amplified detection of aflatoxin B1 using gold nanoparticles as colorimetric indicators. *Nanoscale, 8*(18), 9791–9797.

Fan, X., Xiaolei, Z., Renqiang, Y., Yi, X., Di, K., Alexis, V. B., & Heeger, A. J. (2010). Colorimetric detection of DNA, small molecules, proteins, and ions using unmodified gold nanoparticles and conjugated polyelectrolytes. *Proceedings of the National Academy of Sciences of the United States of America, 107*, 10837–10841.

Freeman, R. G., Grabar, K. C., Allison, K. J., Bright, R. M., Davis, J. A., Guthrie, A. P., ... Walter, D. G. (1995). Self-Assembled Metal Colloid Monolayers: An Approach to SERS Substrates. *Science, 267*(5204), 1629–1632.

Gordon Seymour, S. (2008). Determination of mycotoxins in human foods. *Chemical Society Reviews, 37*(11), 2468–2477.

Hao, N., Lu, J., Zhou, Z., Hua, R., & Wang, K. (2018). A pH-Resolved Colorimetric Biosensor for Simultaneous Multiple Target Detection. *ACS Sensors, 3*(10), 2159–2165.

Huang, Y., Fang, L., Zhu, Z., Ma, Y., Zhou, L., Chen, X., ... Yang, C. (2016). Design and synthesis of target-responsive hydrogel for portable visual quantitative detection of uranium with a microfluidic distance-based readout device. *Biosensors and Bioelectronics, 85*, 496–502.

Huo, Y., Qi, L., Lv, X. J., Lai, T., Zhang, J., & Zhang, Z. Q. (2016). A sensitive aptasensor for colorimetric detection of adenosine triphosphate based on the protective effect of ATP-aptamer complexes on unmodified gold nanoparticles. *Biosensors and Bioelectronics, 78*, 315–320.

Hussein, H. S., & Brasel, J. M. (2001). Toxicity, metabolism, and impact of mycotoxins on humans and animals. *Toxicology, 167*(2), 101–134.

Jv, Y., Li, B., & Cao, R. (2010). Positively-charged gold nanoparticles as peroxidase mimic and their application in hydrogen peroxide and glucose detection. *Chemical Communications (Cambridege, England), 46*(42), 8017–8019.

Kim, H. N., Wen, X. R., Kim, J. S., & Yoon, J. (2012). Fluorescent and colorimetric sensors for detection of lead, cadmium, and mercury ions. *Chemical Society Reviews, 41*(8), 3210–3244.

Ligler, F. S., Taitt, C. R., Shriver-Lake, L. C., Sapsford, K. E., Shubin, Y., & Golden, J. P. (2003). Array biosensor for detection of toxins. *Analytical and Bioanalytical Chemistry, 377*(3), 469–477.

Liu, X., Xu, Y., Wan, D. B., Xiong, Y. H., He, Z. Y., Wang, X. X., ... Hammock, B. D. (2015). Development of a nanobody-alkaline phosphatase fusion protein and its application in a highly sensitive direct competitive fluorescence enzyme immunoassay for detection of ochratoxin A in cereal. *Analytical Chemistry, 87*(2), 1387–1394.

Liu, P., Yang, X., Sun, S., Wang, Q., Wang, K., Huang, J., ... He, L. (2013). Enzyme-free colorimetric detection of DNA by using gold nanoparticles and hybridization chain reaction amplification. *Analytical Chemistry, 85*(16), 7689–7695.

Marin, S., Ramos, A. J., Cano-Sancho, G., & Sanchis, V. (2013). Mycotoxins: Occurrence, toxicology, and exposure assessment. *Food and Chemical Toxicology, 60*, 218–237.

Medley, C. D., Smith, J. E., Zhiwen, T., Yanrong, W., Suwussa, B., & Weihong, T. (2008). Gold nanoparticle-based colorimetric assay for the direct detection of cancerous cells. *Analytical Chemistry, 80*(4), 1067–1072.

Ni, P., Dai, H., Wang, Y., Sun, Y., Shi, Y., Hu, J., & Li, Z. (2014). Visual detection of melamine based on the peroxidase-like activity enhancement of bare gold nanoparticles. *Biosensors and Bioelectronics, 60*, 286–291.

Peng, Y., Li, L., Mu, X., & Guo, L. (2013). Aptamer-gold nanoparticle-based colorimetric assay for the sensitive detection of thrombin. *Sensors And Actuators B-Chemical, 177*, 818–825.

Piermarini, S., Micheli, L., Ammida, N. H., Palleschi, G., & Moscone, D. (2007). Electrochemical immunosensor array using a 96-well screen-printed microplate for aflatoxin B1 detection. *Biosensors and Bioelectronics, 22*(7), 1434–1440.

Rubert, J., Soler, C., Marín, R., James, K. J., & Mañes, J. (2013). Mass spectrometry strategies for mycotoxins analysis in European beers. *Food Control, 30*(1), 122–128.

Sforza, S., Dall'asta, C., & Marchelli, R. (2006). Recent advances in mycotoxin determination in food and feed by hyphenated chromatographic techniques/mass spectrometry. *Mass Spectrometry Reviews, 25*(1), 54–76.

Shephard, G. S. (2008). Determination of mycotoxins in human foods. *Chemical Society Reviews, 37*(11), 2468–2477.

Soleas, G. J., Yan, J., & Goldberg, D. M. (2001). Assay of ochratoxin A in wine and beer by high-pressure liquid chromatography photodiode array and gas chromatography mass selective detection. *Journal of Agricultural and Food Chemistry, 49*(6), 2733.

Song, Y., Wei, W., & Qu, X. (2011). Colorimetric biosensing using smart materials. *Advanced Materials, 23*(37), 4215–4236.

Tang, L., Wang, Y., Liu, Y., & Li, J. (2011). DNA-directed self-assembly of graphene oxide with applications to ultrasensitive oligonucleotide assay. *ACS Nano, 5*(5), 3817.

Thomas, K., Wechsler, D., Chen, Y. M., Crain, S., & Quilliam, M. A. (2016). Analysis of natural toxins by liquid chromatography-chemiluminescence nitrogen detection and application to the preparation of certified reference materials. *Journal of AOAC International, 99*(5), 1173–1184.

Wang, C., Qian, J., Wang, K., Wang, K., Liu, Q., Dong, X., ... Huang, X. (2015). Magnetic-fluorescent-targeting multifunctional aptasensorfor highly sensitive and one-step rapid detection of ochratoxin A. *Biosensors and Bioelectronics, 68*, 783–790.

Wang, C., Qian, J., Wang, K., Yang, X., Liu, Q., Hao, N., ... Huang, X. (2016). Colorimetric aptasensing of ochratoxin A using Au@Fe3O4 nanoparticles as signal indicator and magnetic separator. *Biosensors and Bioelectronics, 77*, 1183–1191.

Wang, J., Shan, Y., Zhao, W. W., Xu, J. J., & Chen, H. Y. (2011). Gold nanoparticle enhanced electrochemiluminescence of CdS thin films for ultrasensitive thrombin detection. *Analytical Chemistry, 83*(11), 4004–4011.

Xu, Z., Hou, Y., & Sun, S. (2007). Magnetic core/shell Fe3O4/Au and Fe3O4/Au/Ag nanoparticles with tunable plasmonic properties. *Journal of the American Chemical Society, 129*(28), 8698–8699.

Xue, Z., Yin, B., Wang, H., Li, M., Rao, H., Liu, X., ... Lu, X. (2016). An organic indicator functionalized graphene oxide nanocomposite-based colorimetric assay for the detection of sarcosine. *Nanoscale, 8*(10), 5488–5496.

Yu, Y., Hong, Y., Gao, P., & Nazeeruddin, M. K. (2016). Glutathione Modified Gold Nanoparticles for Sensitive Colorimetric Detection of Pb(2+) Ions in Rainwater Polluted by Leaking Perovskite Solar Cells. *Analytical Chemistry, 88*(24), 12316–12322.

Zhang, S., Li, H., Wang, Z., Liu, J., Zhang, H., Wang, B., & Yang, Z. (2015). A strongly coupled Au/Fe3O4/GO hybrid material with enhanced nanozyme activity for highly sensitive colorimetric detection, and rapid and efficient removal of Hg(2+) in aqueous solutions. *Nanoscale, 7*(18), 8495–8502.

Zhao, Y., Zhang, X. B., Han, Z. X., Qiao, L., Li, C. Y., Jian, L. X., ... Yu, R. Q. (2009). Highly sensitive and selective colorimetric and off-on fluorescent chemosensor for Cu2+ in aqueous solution and living cells. *Analytical Chemistry, 81*(16), 7022–7030.

Zhou, Z., Hao, N., Zhang, Y., Hua, R., Qian, J., Liu, Q., ... Wang, K. (2017). A novel universal colorimetric sensor for simultaneous dual target detection through DNA-directed self-assembly of graphene oxide and magnetic separation. *Chemical Communications, 53*(52), 7096–7099.

Zhou, Z., Wei, W., Zhang, Y., & Liu, S. (2013). DNA-responsive disassembly of AuNP aggregates: Influence of nonbase-paired regions and colorimetric DNA detection by exonuclease III aided amplification. *Journal of Materials Chemistry B, 1*(22), 2851–2858.